ELSEVIER

Journal of Applied Geophysics 45 (2000) 239–259

JOURNAL OF APPLIED GEOPHYSICS

www.elsevier.nl/locate/jappgeo

# Comparison of methods for estimating earth resistivity from airborne electromagnetic measurements

Les P. Beard *

*Geological Survey of Norway, Leiv Eirikssons vei 39 N-7491 Trondheim, Norway*

Received 3 May 2000; accepted 25 September 2000

**Abstract**

Earth resistivity estimates from frequency domain airborne electromagnetic data can vary over more than two orders of magnitude depending on the half-space estimation method used. Lookup tables are fast methods for estimating half-space resistivities, and can be based on in-phase and quadrature measurements for a specified frequency, or on quadrature and sensor height. Inverse methods are slower, but allow sensor height to be incorporated more directly. Extreme topographic relief can affect estimates from each of the methods, particularly if the portion of the line over the topographic feature is not at a constant height above ground level. Quadrature–sensor height lookup table estimates are generally too low over narrow valleys. The other methods are also affected, but behave less predictably. Over very good conductors, quadrature–sensor height tables can yield resistivity estimates that are too high. In-phase–quadrature tables and inverse methods yield resistivity estimates that are too high when the earth has high magnetic susceptibility, whereas quadrature–sensor height methods are unaffected. However, it is possible to incorporate magnetic susceptibility into the in-phase–quadrature lookup table. In-phase–quadrature lookup tables can give different results according to whether the tables are ordered according to the in-phase component or the quadrature component. The rules for handling negative in-phase measurements are particularly critical. Although resistivity maps produced from the different methods tend to be similar, details can vary considerably, calling into question the ability to make detailed interpretations based on half-space models. 

*Keywords:* Airborne electromagnetic survey; Resistivity; Inversion; Lookup table

## 1. Introduction

Numerous case studies attest to the fact that airborne electromagnetic (AEM) systems have reached a level of sensitivity such that they are no longer simply anomaly finders in the search for massive sulfide ores, but can be reliably used for earth resistivity mapping (Palacky, 1986). AEM resistivity mapping can thus serve as a major component in a wide variety of geological, engineering, and hydrological investigations. Making a resistivity map from airborne data requires careful data collection and painstaking data processing, but the reward is map that can be quantitatively connected to rock properties, and that has the effect of sensor height removed, unlike maps showing in-phase or quadrature measurements. It is thus fair to ask to what degree

* Fax: +47-73-904494.
*E-mail address:* Les.Beard@ngu.no (L.P. Beard).

0926-9851/00/$ - see front matter 
PII: S0926-9851(00)00032-X

resistivity estimates obtained from AEM data can be trusted.

A variety of methods exist for estimating earth resistivity from frequency domain AEM measurements, but a commonly used subset of methods are those based on a conductive half-space model. Typically, for a specific frequency, the in-phase (IP) and quadrature ($Q$) components and the EM sensor height are used to estimate the earth's resistivity below the sensor. In this paper, three different methods are compared: two use precomputed lookup tables, the third uses linearized, iterative inversion. Methods for AEM interpretation based on neural networks hold promise (Ahl et al., 1999), but are still very much topics of active research and are not considered further in this paper.

A lookup table that uses IP and $Q$ component data is simply a digitized version of a phasor diagram, an example of which is shown in Fig. 1. The success of the IP–$Q$ phasor diagram rests on the fact that for a given IP and $Q$ measurement at a particular frequency and transmitter–receiver coil separation, there exists exactly one half-space resistivity and sensor height that fits the measurement. Conversion of the phasor diagram to a lookup table is not a particularly difficult task, but some details are worth mentioning and will be discussed in Section 3.

It is not uncommon for airborne systems to have problems with the in-phase component. The IP component is susceptible to aircraft-generated noise, and over magnetically susceptible rocks the magnitude of the IP can be substantially decreased (Ward, 1961;

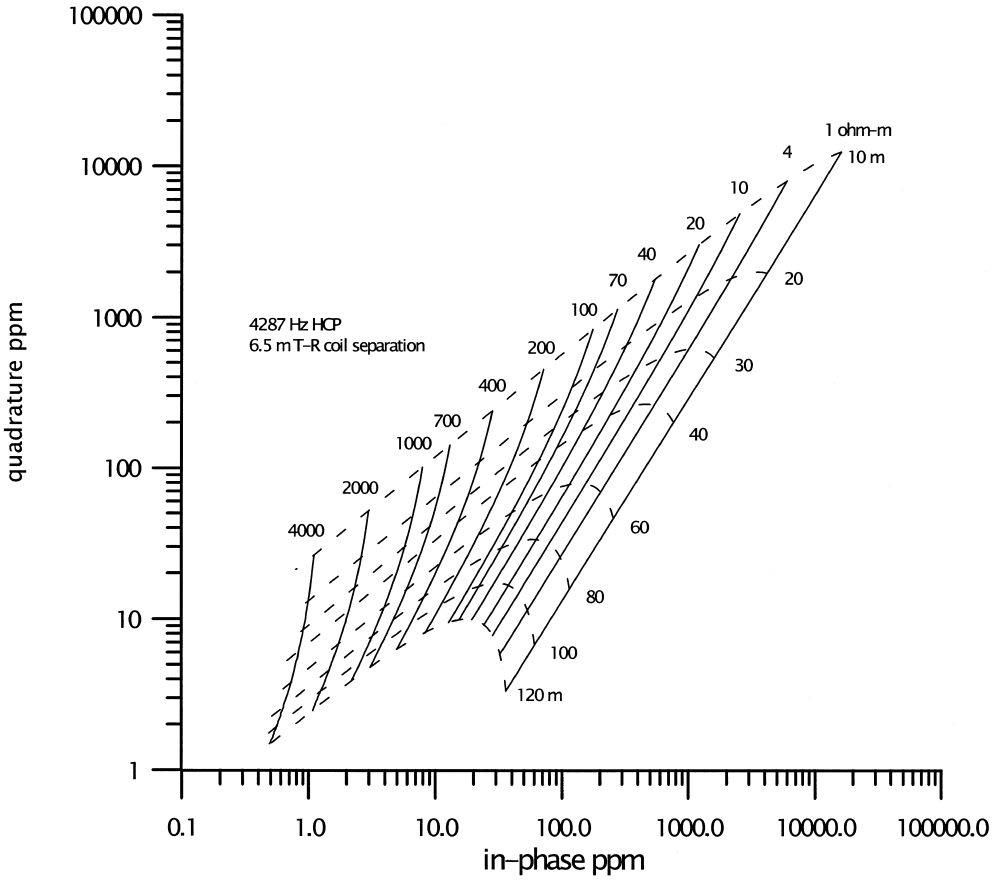


Fig. 1. Phasor diagram for a 4287-Hz HCP system with 6.5-m coil separation. The diagram is valid for half-space resistivities between 1 and 4000 Ω m and for sensor heights between 10 and 120 m.

Fraser, 1981). In situations where the reliability of IP data is questionable, the half-space resistivity can be estimated using lookup tables created from the $Q$ component and the measured sensor height ($H$). However, the $Q$–$H$ method for resistivity estimation suffers from the problem of non-uniqueness. Fig. 2 shows a plot of EM response as a function of conductivity for a horizontal coplanar system operating at 4287 Hz with a 6.5-m transmitter–receiver coil spacing, denoted System A in further discussion. There are two half-space conductivities that can produce a given $Q$ response. Fortunately, for the parameters used by most AEM systems, the peak of the $Q$ curve, marked 'Cutoff' in Fig. 2, occurs at a high conductivity, in this particular case at 300 mS/m (3.33 Ω m). For resistivity mapping, the low conductivity solution is usually preferred. When constructing $Q$–$H$ lookup tables, all conductivities to the right of the peak are excised, forcing the solution to be unique, but skewed to lower conductivities.

In comparison with lookup tables, linearized least-squares inversion is much more computationally intensive. Whereas earth resistivity estimates for a moderate size survey of a few thousand line-kilometers can be processed in a few minutes using a lookup table, inverse methods can take hours. Many types of inversion schemes require an initial estimate of ground conductivity, and solutions can sometimes be dependent on this initial estimate. However, linearized inversion possesses some advantages over lookup tables. The IP and $Q$ components can be given different weightings in a Marquardt-type inversion scheme (Menke, 1984). Low quality data can thus be given a lower weight rather than being discarded completely. This is also possible in principle with IP–$Q$ lookup tables, but is usually not done. Inversion schemes use sensor height data more directly than IP–$Q$ lookup tables, and it is easy to incorporate resistivity and sensor height bounds into inversion algorithms, thus giving a measure of control over the range of possible solutions.

These three methods for estimating earth resistivity are different enough from one another that it should not be surprising if they produce somewhat different estimates. Each method has its own strong and weak points. By better understanding these strengths and weaknesses, the processor of AEM data can better match the method to the circum-

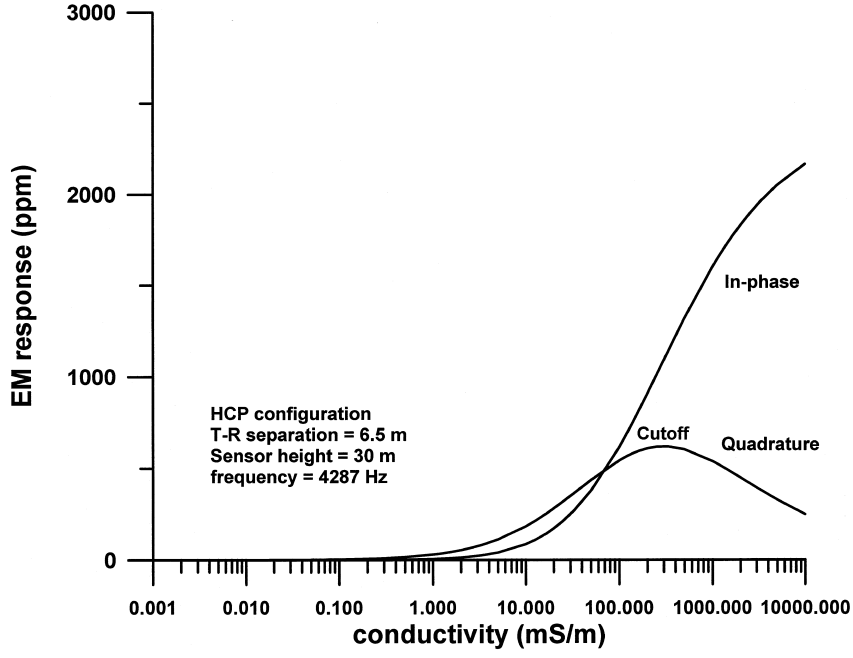


Fig. 2. In-phase and quadrature response as a function of conductivity.

stances of a given survey, and the interpreter of the data can better judge which anomalies are real and which are artifacts of a particular estimation scheme.

## 2. EM response of a homogeneous half-space

For a loop–loop EM system consisting of horizontal coplanar coils separated by a distance $r$, the mutual impedance ratio $Z/Z_0$ is given by

$$\frac{Z}{Z_0} = 1 + B^3 T_0 \tag{1}$$

where $B = r/\delta$. For a system having angular frequency $\omega$, the skin depth $\delta$ of a uniform earth of conductivity $\sigma$ and free-space magnetic permeability $\mu_0$ and is equal to $\sqrt{2/\omega\mu_0\sigma}$. $Z_0$ is the impedance of the system as measured in free-space. The integral $T_0$ takes the form

$$T_0 = \int_0^\infty R(x)\, x^2 \exp(-Ax)\, J_0(Bx)\, \mathrm{d}x \tag{2}$$

where $A = 2h/\delta$. $J_0$ is the Bessel function of order zero and $h$ is the EM receiver height above ground level. $R(x)$ is a transfer function having the form $R(x) = (x - U)/(x + U)$ where $U = \sqrt{x^2 + j2}$ with $j = \sqrt{-1}$. The mutual impedance ratio $Z/Z_0$ is a complex number whose real part represents the in-phase response of the system and whose imaginary component is the quadrature response. Eq. (1) is used to generate lookup tables and also in the forward computations used in half-space inversion algorithms. For multiple layer earth models, recursion formulae can be found in Wait (1982). Beard and Nyquist (1998) give formulae for one- and two-layered magnetic earth models ($\mu \geq \mu_0$).

## 3. Construction of lookup tables

Lookup tables can be constructed from phasor diagrams for a variety of simple models—spheres, horizontal thin sheets, or half-spaces. In this paper, only the conductive half-space model is considered. Lookup table parameters can also vary (Telford et al., 1990, chapter 7), but in this paper are confined to two commonly used combinations: quadrature and in-phase ($Q$–IP) or quadrature and sensor height ($Q$–$H$). Also note, a $Q$–IP table is ordered by increasing quadrature and an IP–$Q$ table is ordered by increasing in-phase response. The $Q$–$H$ method is doubly ordered, initially by increasing sensor height, then for a given sensor height, by decreasing quadrature response.

### 3.1. Q–IP lookup tables

A phasor diagram consists of a set of non-intersecting curves plotted as a function of in-phase and quadrature response. As is shown in Fig. 1, each curve corresponds to a unique half-space resistivity and is constructed by computing the IP and $Q$ responses as a function of system height above the surface of the half-space. A second set of non-intersecting curves cross the resistivity curves and represent the sensor height. The interpreter selects a $Q$–IP pair from the data set and finds the corresponding resistivity and height by interpolating between curves. This method is good for checking a few points, but whole data sets require the process to be computerized.

Whereas the $Q$–IP phasor diagram is a continuum, a lookup table has necessarily to be discretized. Rules have to be formulated so that if a particular measured $Q$–IP pair is not found precisely in the table, a reasonable resistivity can still be selected. To create the $Q$–IP table, responses were generated from a single frequency over sensor heights ranging from 10 to 400 m above ground level, and over a resistivity range of 1–40 000 Ω m. Quasi-logarithmic sampling was used for both sensor height and resistivity. The table was then ordered from low to high quadrature response, retaining enough decimal places that none of the quadrature values repeated. This determined the order of the in-phase component, the sensor height and the half-space resistivity. Given a measured pair of in-phase and quadrature values, $\mathrm{IP_M}$ and $Q_\mathrm{M}$, the program searches for $Q^*$, the first $Q$ in the table greater than $Q_\mathrm{M}$. Upon finding $Q^*$, the program searches a specified range of IP, $Q$ pairs centered on $Q^*$, choosing the pair that minimizes

$$(\mathrm{IP} - \mathrm{IP_M})^2 + (Q - Q_\mathrm{M})^2. \tag{3}$$

This choice then determines the sensor height $H$ and the ground resistivity $\rho^*$. Numerical tests

showed that so long as negative IP responses were handled by setting $IP_M$ equal to zero in Eq. (4), a more accurate resistivity estimate could usually be achieved by multiplying the $Q$–IP lookup table resistivity $\rho^*$ by the square root of the ratio of the response amplitudes. Thus,

$$\rho = \sqrt{\left(IP_L^2 + Q_L^2\right)/\left(IP_M^2 + Q_M^2\right)}\,\rho^* \qquad (4)$$

where the subscript L implies lookup table values and M implies measured values. Eq. (4) was used rather than interpolation between adjacent resistivity entries in the lookup table because in the $Q$–IP lookup table adjacent resistivities may vary widely. Adjacent entries in the table may have similar $Q$ and IP values, but these may be computed at very different sensor heights, and therefore are produced by dissimilar earth resistivities. On the other hand, this is not a problem with the $Q$–$H$ lookup table described in Section 3.2, and interpolation can be used successfully in this kind of lookup table.

The sampling interval of the lookup table is important. A table with 10 resistivity entries per decade can be expected to give better results than a table with only two entries per decade. Shown in Fig. 3 are resistivity and sensor height estimates for two different half-space models, a 146-Ω m earth and a 507-Ω m earth. These numbers have been chosen so that the lookup table will not contain the exact value, as it might in the case of a 100-Ω m earth. The lookup tables were constructed for a 4287-Hz horizontal coplanar loop system having a loop separation of 6.5 m (System A) using 2, 3, 5, and 10 resistivities per decade. The 10 per decade table yields very close estimates for both sensor height and resistivity for the 146-Ω m earth, but for the 507-Ω m earth, the two per decade table gives the closest estimate. This happens because the 2 per decade table had a sample point for a 30-m sensor height and a 500-Ωm earth, very near the true sensor height and resistivity. This of course is an exception. Over a wide range of resistivities, the 10 per decade table should be expected to give better estimates.

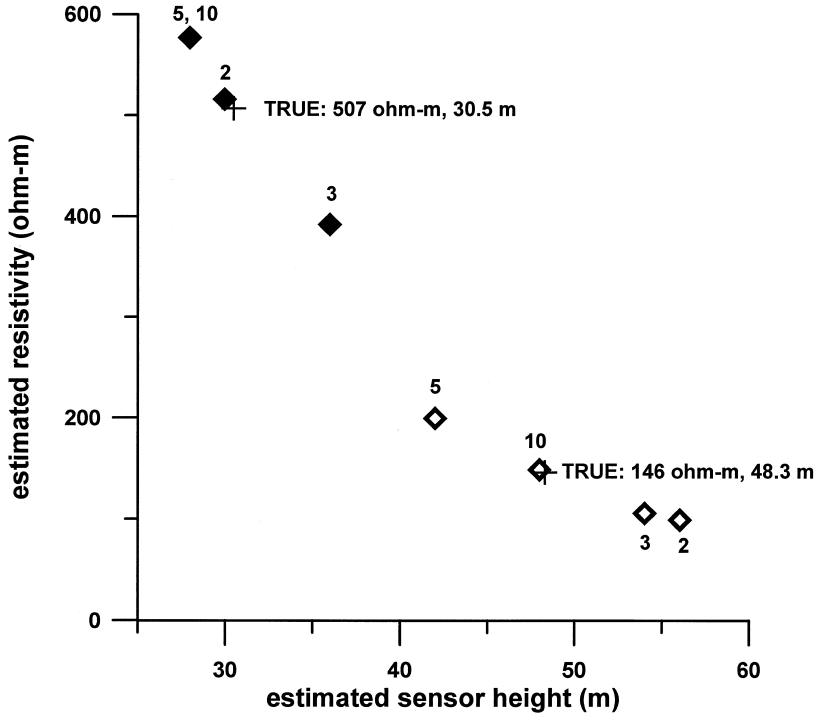


Fig. 3. Effect of lookup table resistivity density (number of sample resistivities per decade) on accuracy of $Q$–IP lookup table solutions for two different half-space models.

The IP component is often the most problematic in a survey, being more affected by the aircraft and by magnetic susceptibility variations. Fig. 4 illustrates the effect of IP discrepancies on the final estimated resistivity and sensor height. In this case, a 997-Ωm earth was sampled at a 30.5-m sensor height for system A. This yields an IP response of 5.7 ppm and a $Q$ response of 29.4 ppm. Leaving the $Q$ response at 29.4 ppm, the IP component was varied from its true value and the resistivity and sensor height was estimated for the incorrect IP and correct $Q$. IP responses lower than about 4 ppm resulted in a resistivity estimate of about 2000 Ω m, and a too low sensor height estimate. As the IP increases, the estimated resistivity decreases and the sensor height estimate increases in steps. Accurate measurement of in-phase and quadrature response and careful leveling are thus essential to obtaining accurate resistivity estimates.

The $Q$–IP lookup table described above is ordered according to ascending $Q$ values. It is reasonable to ask if the same results are obtained if the table is organized according to ascending IP. As is shown in this article, if appropriate rules for handling negative IP measurements are developed, maps made from either method are similar, though not exact, and if negative IP is handled poorly, very inaccurate IP–$Q$ estimates can result.

### 3.2. Q–H lookup tables

Construction of a lookup table based on quadrature and sensor height is straightforward. For a par-

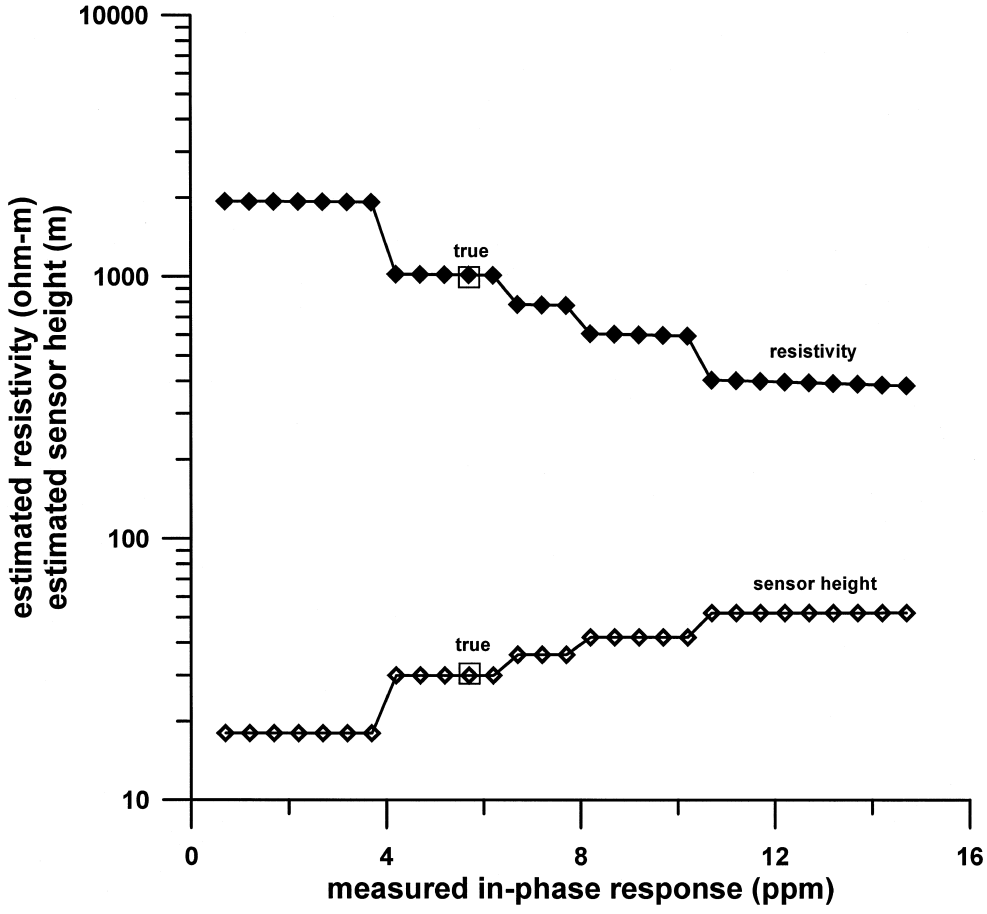


Fig. 4. Effect of incorrectly leveled in-phase response on resistivity and sensor height estimates from a $Q$–IP lookup table.

ticular sensor height, the quadrature response is computed for a wide range of resistivities. The table is doubly ordered, first according to increasing sensor height, then for a given sensor height, according to decreasing quadrature response. Given a measured sensor height and quadrature response, a search is performed to find the nearest tabulated sensor height. Then, a search is conducted over the tabulated quadrature responses at this height to find the responses $Q_i$ and $Q_{i+1}$ (and associated resistivities $\rho_i$ and $\rho_{i+1}$) that bracket the measured response $Q_M$. An interpolation is then performed to get the estimated resistivity $\rho$:

$$\rho = \rho_i + (\rho_{i+1} - \rho_i) * (Q_i - Q_M)/(Q_i - Q_{i+1}). \quad (5)$$

The success of this method requires that low resistivities beyond the cutoff resistivity (see Fig. 2) have been excised from the table; otherwise the solution would be non-unique. It is also dependent on the accuracy of the measured sensor height. Fig. 5 illustrates what can happen to the half-space resistivity estimate if the measured sensor height is in error. The response of System A was computed for a sensor height of 32.6 m and half-space resistivities of 38 and 861 Ω m. The diamonds show how resistivity estimates change if the measured sensor height is inaccurate. Measured sensor heights that are lower than the true value lead to resistivity estimates that are too high; those higher than the true height result in resistivity estimates that are too low. The variation in estimate for the high resistivity model is fairly regular. The unusual behavior in the low resistivity model estimates beyond sensor heights of about 40 m occurs because the cutoff resistivity has been reached for that particular height. No lower estimates

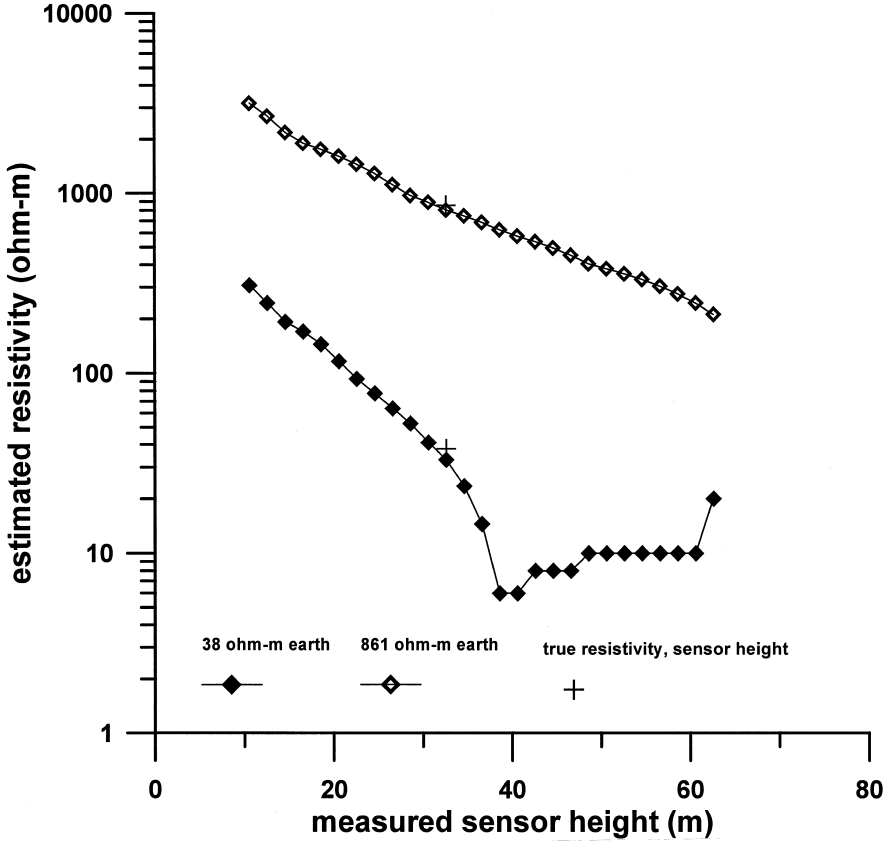


Fig. 5. Effect of incorrectly measured sensor height on $Q$–$H$ lookup table resistivity estimates for two different half-space models.

are possible. Furthermore, the cutoff resistivity is progressively higher for increasing sensor heights, thus the upward stairstep pattern as sensor height increases.

## 4. Marquardt–Levenburg inversion

The earth's resistivity can be estimated from a single frequency of AEM data by using damped, iterative least-squares inversion. In this study, the Marquardt–Levenburg method (Marquardt, 1963; Press et al., 1992) is used, an approach that is relatively fast and robust for the modest sized matrices encountered in computing resistivity from a single AEM frequency. In this case, the inverse problem is even determined, having only two data values —the in-phase and quadrature components at a single position and frequency—and two unknowns, the half-space resistivity and the sensor height. Both unknowns can be constrained to lie within specified limits. Although the sensor height is actually a measured quantity, it can be in error in areas of rugged terrain or in densely vegetated regions. Even in areas where the sensor height is trusted, additional geophysical information, e.g. overburden thickness, can often be obtained by leaving it as an inversion parameter (Hogg and Boustead, 1990).

In this study a two-point data vector $\boldsymbol{d}$, consisting of the in-phase and quadrature measurements at a single frequency computed from the half-space model described above, are non-linearly related to the model's parameter vector $\boldsymbol{m}$ (the half-space resistivity and sensor height). The Marquardt–Levenburg method assumes a linear relationship exists over a small neighborhood of solution space and relates $\boldsymbol{d}$ and $\boldsymbol{m}$ by the matrix equation

$$\boldsymbol{d} = \mathbf{A}\boldsymbol{m} \tag{6}$$

where $\mathbf{A}$ is a $2 \times 2$ matrix whose elements $A_{ij}$ take the form $\partial d_i/\partial m_j$. Eq. (6) can be solved iteratively by choosing an initial parameter estimate $\boldsymbol{m}_0$ then computing a change $\delta\boldsymbol{m}$ in the parameter vector that serves to reduce the difference between the computed data vector and the observed data $\boldsymbol{d}^{\text{obs}}$ in a least-squares sense. $\delta\boldsymbol{m}$ can then be obtained from a regularized solution of Eq. (6):

$$\delta\boldsymbol{m} = (\mathbf{A}^{\mathrm{T}}\mathbf{A} + \lambda^2\mathbf{I})^{-1}\mathbf{A}^{\mathrm{T}}(\boldsymbol{d}^{\text{obs}} - \boldsymbol{d}). \tag{7}$$

In Eq. (7), the term $\lambda^2\mathbf{I}$ represents a weighting matrix necessary for solution stability. $\lambda^2$ is called the damping factor and helps control how rapidly a solution changes from one iteration to the next. For a particular iteration $i$, the improved solution is $\boldsymbol{m}_{i+1} = \boldsymbol{m}_i + \delta\boldsymbol{m}$. The updated solution is inserted into Eq. (6) and the iterative process continues until $\boldsymbol{d}^{\text{obs}} - \boldsymbol{d}$ becomes sufficiently small or until a predetermined number of iterations has been exceeded.

## 5. Comparisons using real and synthetic data

In this section, the different solutions described above are compared using both real and synthetic data. First, layered earth synthetic models and 3-D synthetics are examined, then estimates from real data are considered.

### 5.1. Two-layer earth models

The in-phase and quadrature components are unique only for a homogeneous half-space. For even a two-layer earth model, solutions are non-unique (Frischknecht et al., 1991). The response of System A at a sensor height of 30.5 m was computed for the three different two-layer earth models described in Fig. 6. The resistivity was then estimated using an $Q$–IP lookup table, a $Q$–$H$ lookup table, and two variants of least-squares inversion. In the inversion denoted as Inv1 in Fig. 6, the sensor height was held fixed at its measured value and only the resistivity was inverted for, and in the second method (Inv2), both the sensor height and resistivity were allowed to vary up to 100% of the measured sensor height. In the case of a conductive layer overlying a more resistive half-space, the resistivities from the different methods are more scattered than for the case of a resistive layer on top of a conductive half-space. If in the latter case the top layer is somewhat magnetic as well, the in-phase response is decreased (in this case by 18 ppm). Resistivity estimation methods that use

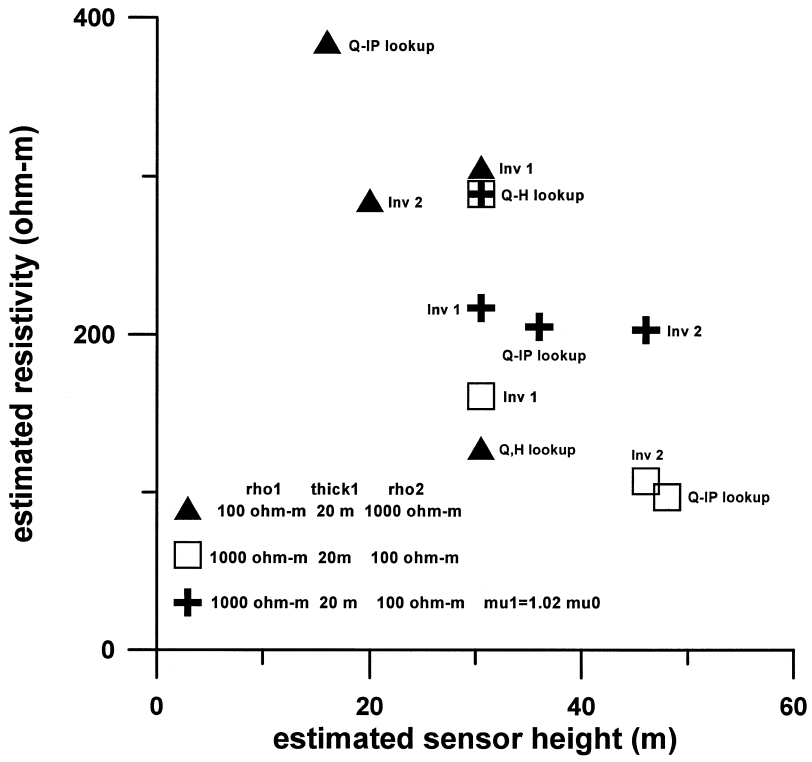


Fig. 6. Resistivity and sensor height estimates from four different methods and three different earth models. Inversion method Inv1 uses the measured sensor height and inverts only for resistivity. Inv2 inverts for both sensor height and resistivity.

the IP component without taking into account magnetic susceptibility are thus likely to estimate the earth resistivity higher than in the non-magnetic case. As can be seen in Fig. 6, the *Q*–IP lookup method and both inversion methods predicted higher resistivities over the magnetic earth than over the same two-layer non-magnetic earth. The *Q–H* method gave the same estimate in both cases because the *Q* component is unchanged by increased magnetic susceptibility.

### *5.2. Topographic effects*

The effects of topography on dipole source EM ground surveys have been documented (Mitsuhata, 2000), and it is reasonable to expect topographic effects to show up in airborne EM surveys as well. Flying draped surveys, where the sensor maintains a constant height above ground level, can be expected to reduce topographic effects in AEM surveys, but in rugged terrain draping can be difficult to achieve. In particular, draping may be dangerous or impossible over narrow valleys. To examine the effects of a valley on resistivity estimation schemes, the response of a long narrow valley cut into an otherwise homogeneous 523-Ω m half-space (Fig. 7a) was modeled using EMIGMA 3-D electromagnetic modeling software. The valley is 10-km long, 1-km wide, and 100-m deep. Outside the valley, the sensor height is 42.8 m above ground level. The sensor does not dip down over the valley, but maintains a level flight path, so that over the valley floor it is at a height of 142.8 m. Shown in Fig. 7b are the measured sensor height and the in-phase and quadrature responses for this model. A homogeneous 523-Ω m earth produces an in-phase response of 10.5 ppm and a quadrature response of 32 ppm in System A at a height of 42.8 m. At 142.8 m, the flat earth IP and *Q* responses

drops to 3 and 4 ppm, respectively. Over the valley, the IP and $Q$ responses decrease, but do not fall to the levels of a flat earth because the earth material outside the valleys keeps the response somewhat elevated.

Shown in Fig. 7c are curves representing the estimated half-space resistivities from the three different methods described above. The most striking result is that of the $Q$–$H$ estimation method. The valley appears as a conductive feature of about 80 Ω

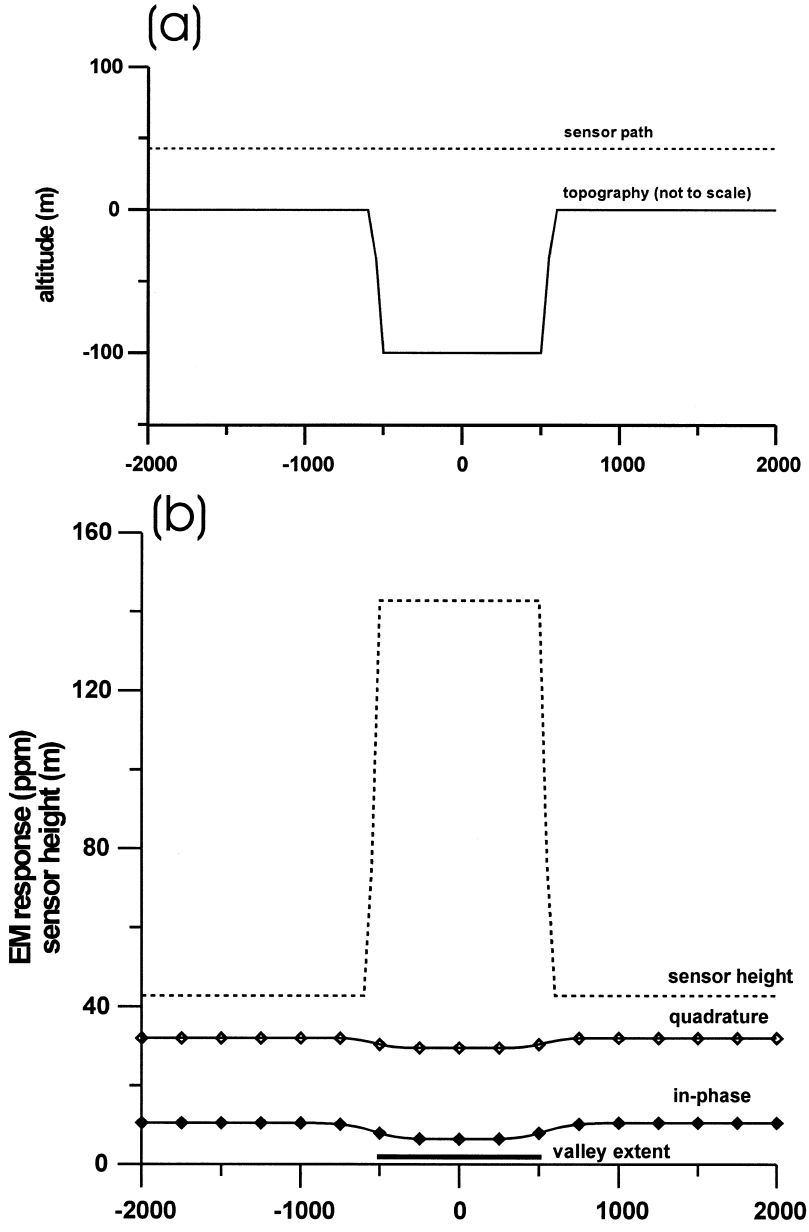


Fig. 7. Synthetic 3D valley model. (a) Valley cross-section and sensor path. (b) Measured parameters. (c) Estimated resistivities from three different methods.

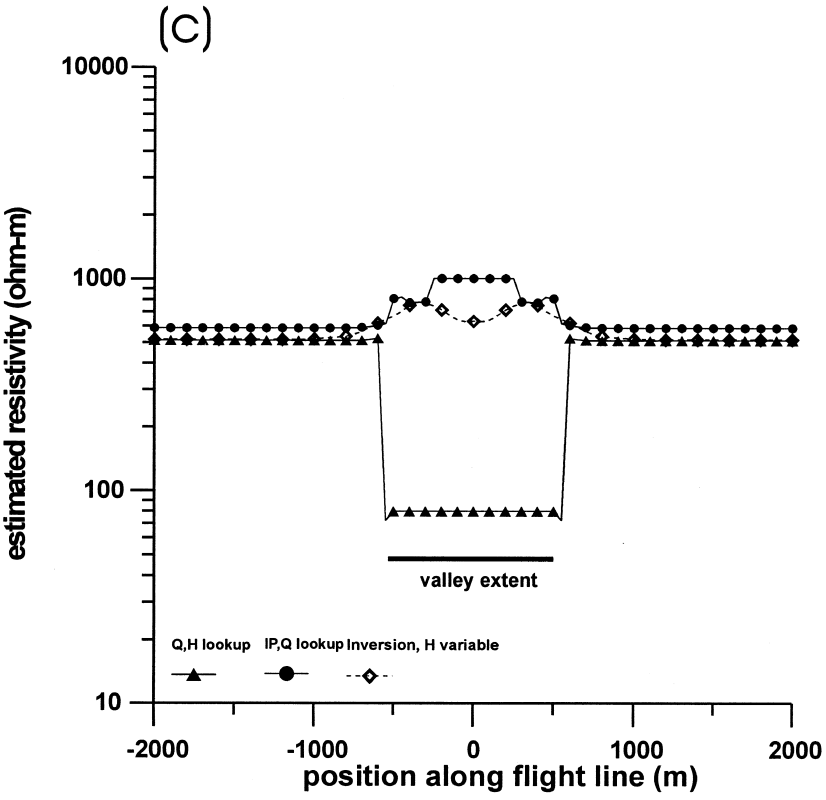


Fig. 7 (*continued*).

m, considerably smaller than the true 523-Ω m resistivity. This occurs because the quadrature response remains well above the 4 ppm level of a 523-Ω m flat earth at a 142.8-m sensor height. The measured sensor height is considered accurate and is unchanged in the *Q*–*H* lookup method, so the elevated quadrature response results in a resistivity estimate that is too low. The *Q*–IP lookup method and the inversion method yield estimates over the valley that are somewhat higher than the 523-Ω m level. The *Q*–IP lookup method as used here first found the quadrature value in the table that was closest to the measured value, then searched a range of quadrature and in-phase values near that point that gave the closest fit in a least-squares sense. No consideration is given to sensor height in this algorithm. Over the center of the valley, the resistivity estimate is about 1000 Ω m, making the valley appear more resistive than the true value. The best fitting solution in the table was a 1000-Ω m earth with a sensor height of 30 m. Because the inverse method also uses a least-squares criterion, it yielded results similar, but not identical to the *Q*–IP lookup method because in the inverse method the sensor height is allowed to vary as an inversion parameter over a limited range, and because the solution space is continuous, rather than discrete as in a lookup table. The estimated sensor height from the inversion algorithm was allowed to vary no more than 100% of the measured sensor height. The inversion results shown in Fig. 7c have been smoothed. Three-dimensional effects from the valley walls caused very high and low spikes in the inverse solution. However, these same points usually show high root-mean-square (RMS) error, and so can be identified as poor estimates. RMS error is not generally computed in lookup table solutions, so identification of poor estimates is more qualitative. Although in this instance the inverse method produced a modest resistivity high over the valley, this should not be generalized.

Inversion results can vary depending on the initial guess and on 3-D effects from local geology and topography.

An examination of real data confirms the results obtained from the synthetic valley model. Shown in Fig. 8a is a topographic cross-section along a 2-km portion of a flight line over volcanic extrusives in the Oslo igneous province. Near the center of the profile is a steep-sided valley about 60-m deep and 200-m wide. The narrowness of the valley prevented the helicopter from draping the EM sensor over the valley, but instead flew directly over it, as can be seen by the increased measured sensor height over the valley in Fig. 8b. The valley is floor is a basaltic

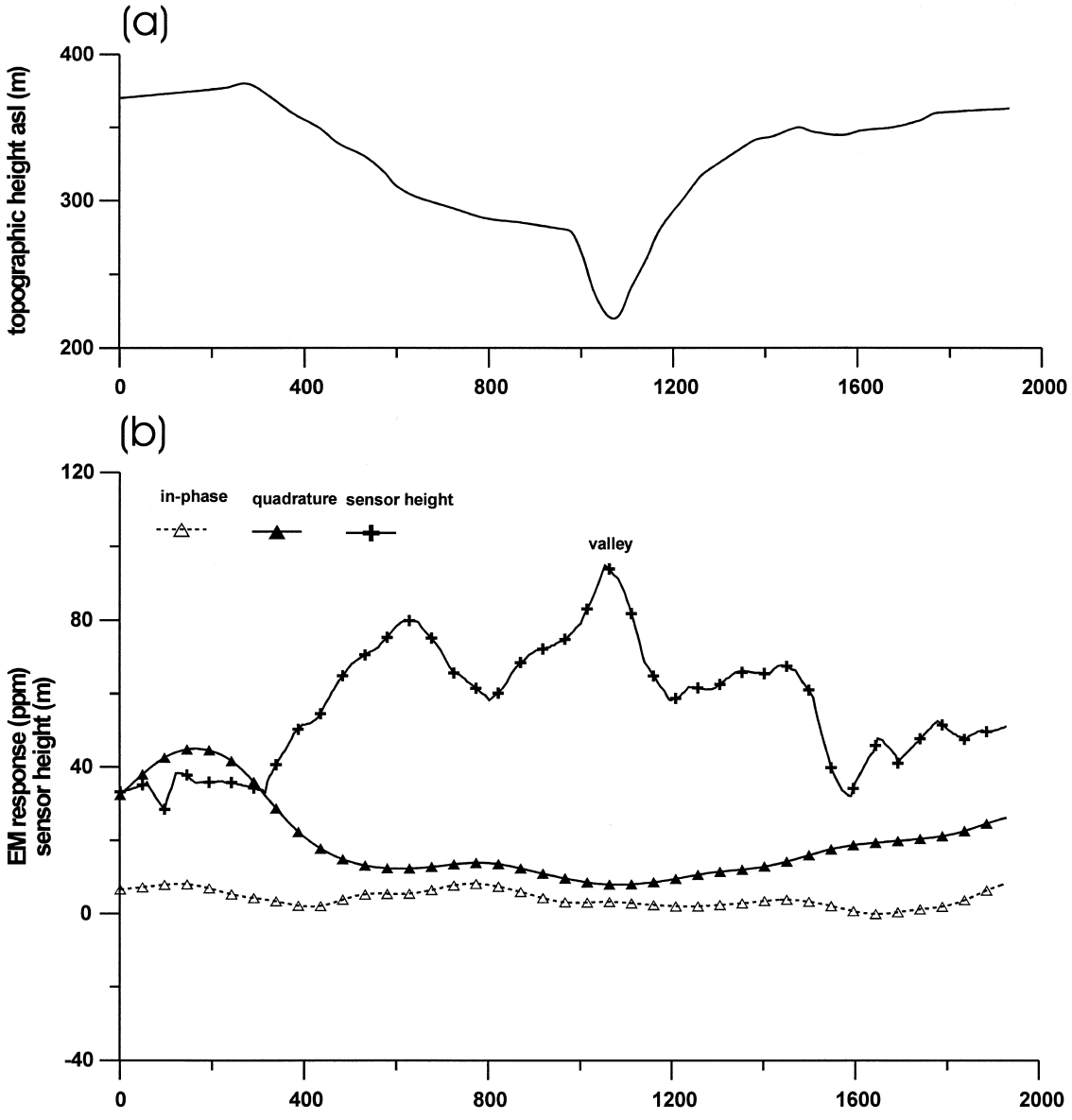


Fig. 8. Field data over valley. (a) Topographic cross-section of valley. (b) Measured parameters. (c) Resistivity estimates from three different methods.

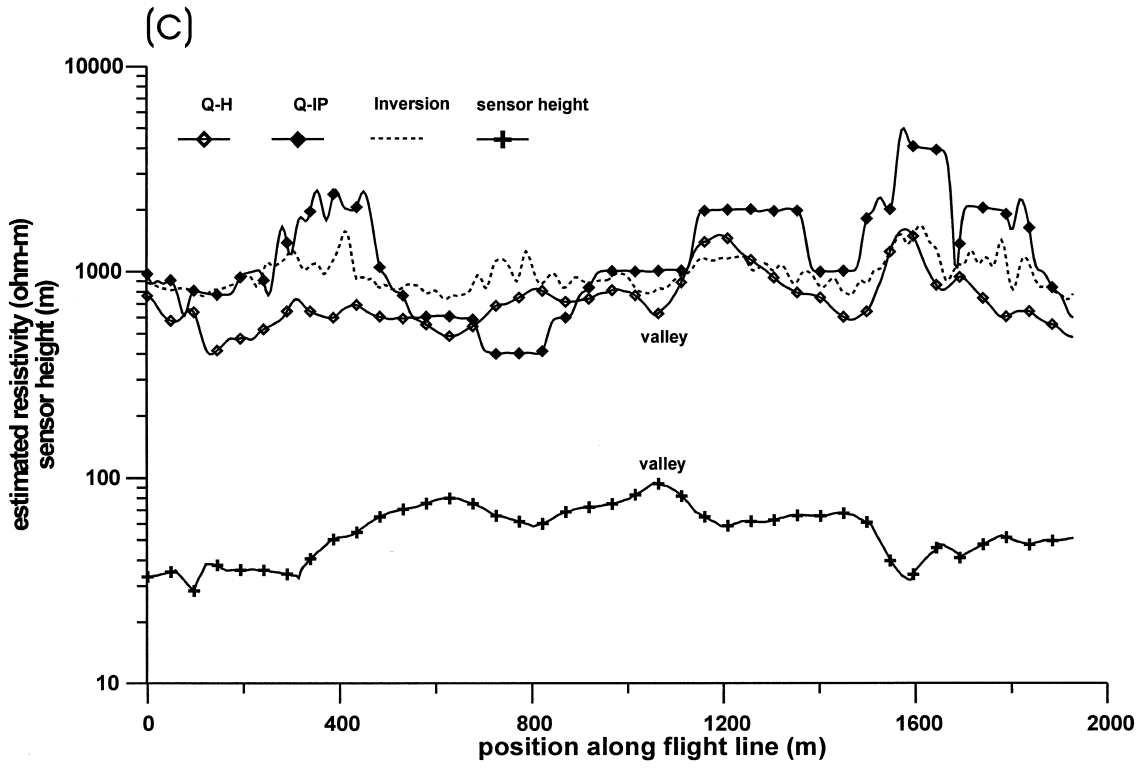


Fig. 8 (*continued*).

unit that is not expected to be greatly different in electrical properties from the lava flows occurring on either side, but a small stream flows along the valley floor that could conceivably produce a decrease in resistivity. A slight drop in the quadrature component takes place over the valley whereas the in-phase is only slightly changed. In Fig. 8c, the *Q–H* lookup table estimate shows a decrease in resistivity over the valley. The *Q*–IP lookup method shows no change over the valley. Inversion results show a small resistivity low over the valley.

To ask which of the three curves in Figs. 7c or 8c is correct is probably an ill-posed question. Each method tries to fit the response due to 3-D geology and topography to an earth model that is altogether too simple—a homogeneous, flat earth. Each method finds a solution according to different rules and so we get three different curves. The good news is that over the 2-km length of the flight line, the curves show general agreement in terms of locations of resistivity highs and lows. An exception occurs at $x = 800$ m where the *Q*–IP method produces a pronounced resistivity low and the other two methods do not.

### 5.3. Resistivity estimates over very good conductors

Another situation in which the *Q–H* method can be expected to give quite different results in comparison with the other methods is when a flight line passes over a very good conductor. As can be seen in Fig. 1, for very high conductivities the quadrature component is small and the in-phase large. Because the *Q–H* method uses only quadrature information skewed to low conductivities, highly conductive structures can be missed with this method. Shown in Fig. 9a is an 8-km segment of a flight line in the Oslo graben. It shows three strong in-phase responses from System A at about $x = 1000$, 2500 and 3000 m. The first two in-phase peaks show hardly any change in the quadrature component. Five different methods were used to estimate half-space resis-

tivity along the line. Least-squares inversion, the $Q$–$H$ lookup method, and three different lookup methods based on IP and $Q$ were compared. As was noted in Section 3, the method labeled IP–$Q$ looks first for the measured IP response in a table ordered according to increasing IP response, then searches the in neighborhood of that value for the closest fitting quadrature response that in conjunction with its corresponding in-phase response minimizes expression (3). The $Q$–IP lookup method finds the measured $Q$ response in a table ordered by increasing $Q$, and then searches in the neighborhood of this value for the best fitting IP response. Both the $Q$–IP and IP–$Q$ estimates were modified using Eq. (4). The third lookup method used a commercial IP–$Q$ lookup table (Geosoft). The results of these five methods are shown in Fig. 9b. The $Q$–$H$ method failed to detect the conductors at $x = 1000$ m and $x = 2500$ m. It detected the conductor at $x = 3000$ m but estimated its resistivity at over 1000 $\Omega$ m, considerably higher than the other methods.

### 5.4. Plan view maps

Given the difference in results obtained along the single line in Section 5.3, I decided to examine several lines of data and make plan view conductivity maps from the different methods. Fig. 10a–c shows maps of in-phase response, quadrature response, and measured sensor height over lava flows in an area of the Oslo igneous province known as Krokskogen (Larsen, 1978). The lava flows form several nearly flat lying layers, broken by normal faults that trend roughly NNW–SSE. Magnetite is present in varying amounts throughout the lava flows (Everdingen, 1960), suppressing the in-phase response and sometimes forcing it to be negative. The IP and $Q$ data in Fig. 10 have had instrument drift removed through the use of periodic high altitude excursions of the helicopter to determine the instrument's zero level, but no filters have been used to remove small line-to-line errors that still remain. The data show generally higher IP and $Q$ responses in

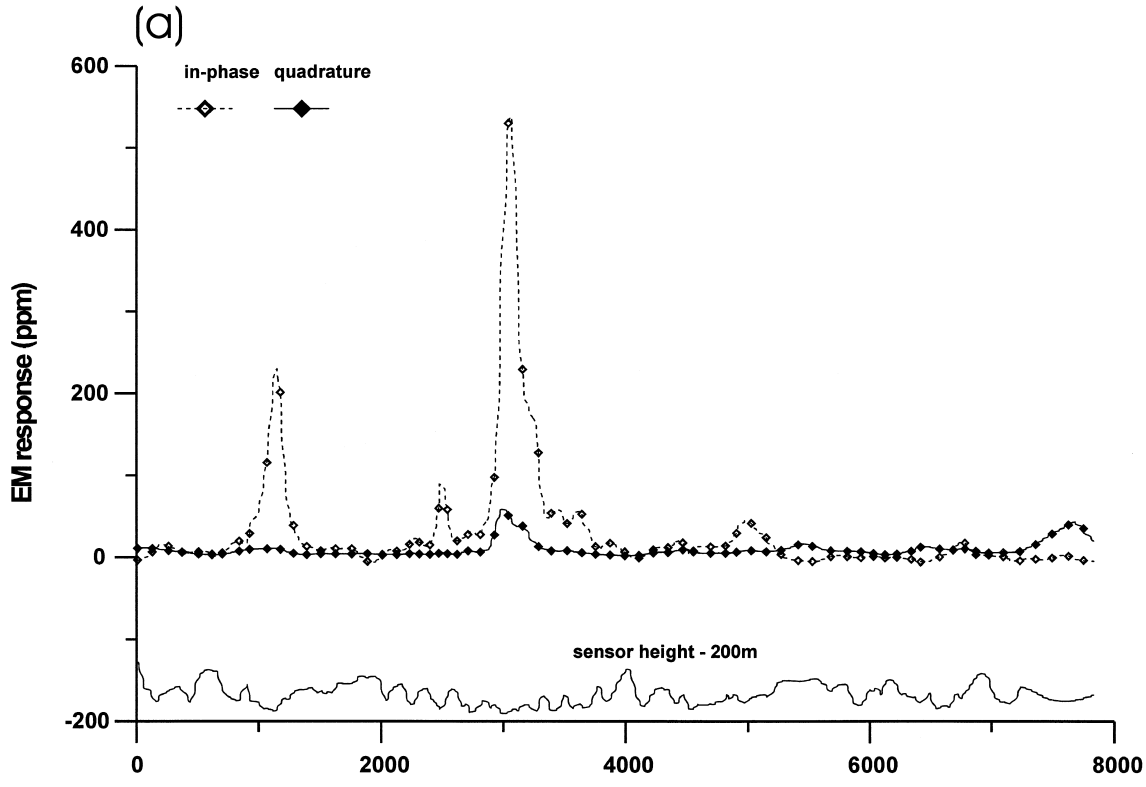


Fig. 9. High conductivity example. (a) Measured data along flight line. (b) Resistivity estimates from five different methods.

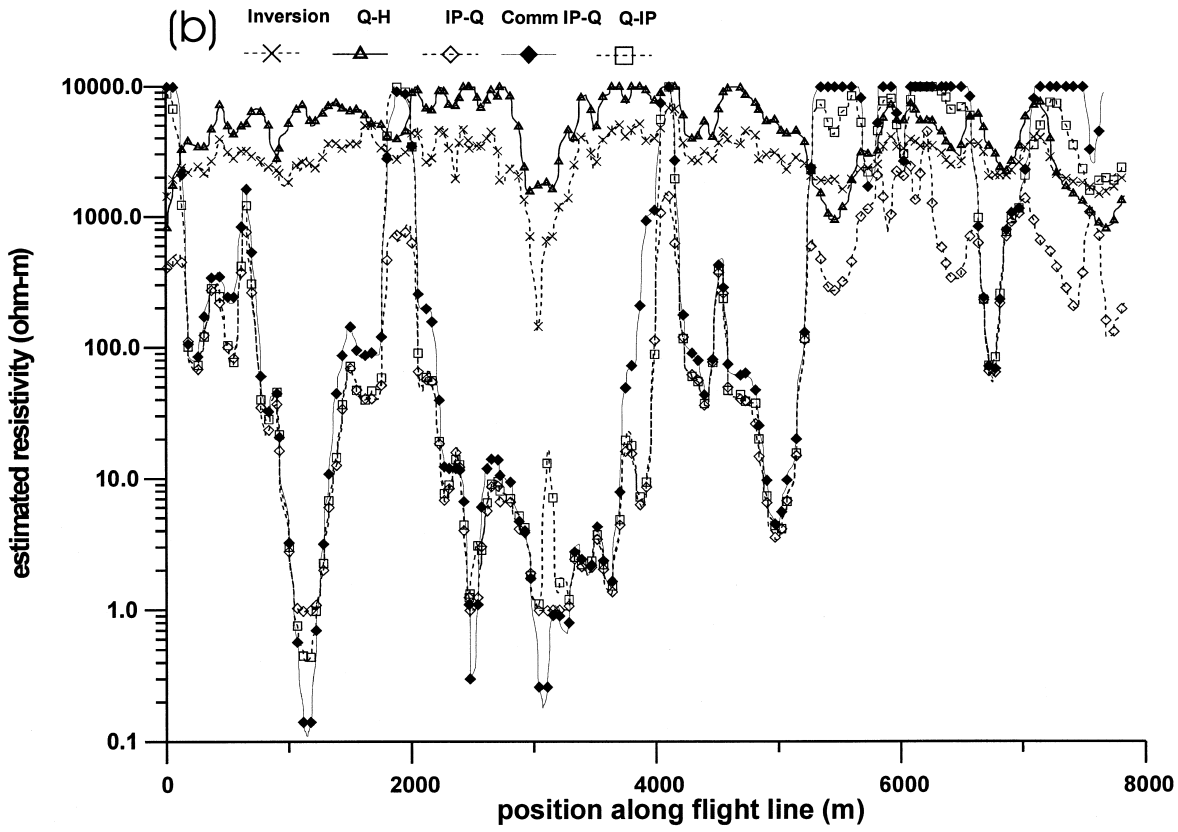


Fig. 9 (*continued*).

the west (left side) than in the east. A zone of high IP and *Q* responses occurs in the center of the area and trends to the SW corner of the area.

Fig. 11 shows six different conductivity estimates: two from least-squares inversion and four from various forms of lookup tables. The color bars for each figure are different in order to emphasize conductivity pattern similarities and differences, rather than absolute conductivity values. Fig. 11a and b shows estimates from inversion. The same algorithm was used for both inversions, but in Fig. 11b the initial damping factor was smaller and the bounds on the permitted sensor height variation were larger, allowing a wider range of possible solutions. In Fig. 11a, the estimated sensor height was allowed to vary only 20% from the measured value, whereas in Fig. 11b it could vary by 100%. The conductivity estimates are quite similar in the two figures, but one small area shows a major difference. The good conductor marked 'X' in Fig. 11a appears as a resistive anomaly in Fig. 11b. Can both these solutions fit the data equally well? At location X, the in-phase component measures 31 ppm, the quadrature component 21 ppm, and the sensor height is 56 m. The inverse solution at point X in Fig. 11a is a 46-Ω m earth with a sensor height of 46 m. The inverse solution in Fig. 11b is a 7000-Ω m earth with a sensor height of 5.6 m. Given that the data are of good quality, there are at least two possible causes for the extremely low estimated sensor height of 5.6 m: a magnetic earth or 3-D effects. In this case, it is probably a combination of both; solutions in the vicinity of X exhibit high RMS error in both inversions.

Fig. 11c shows conductivity estimates from the *Q*–IP lookup table method. The pattern is similar to that of the inversion estimates. The main difference is that the low conductivity zone that appears in the center right side of the inversion figures is not

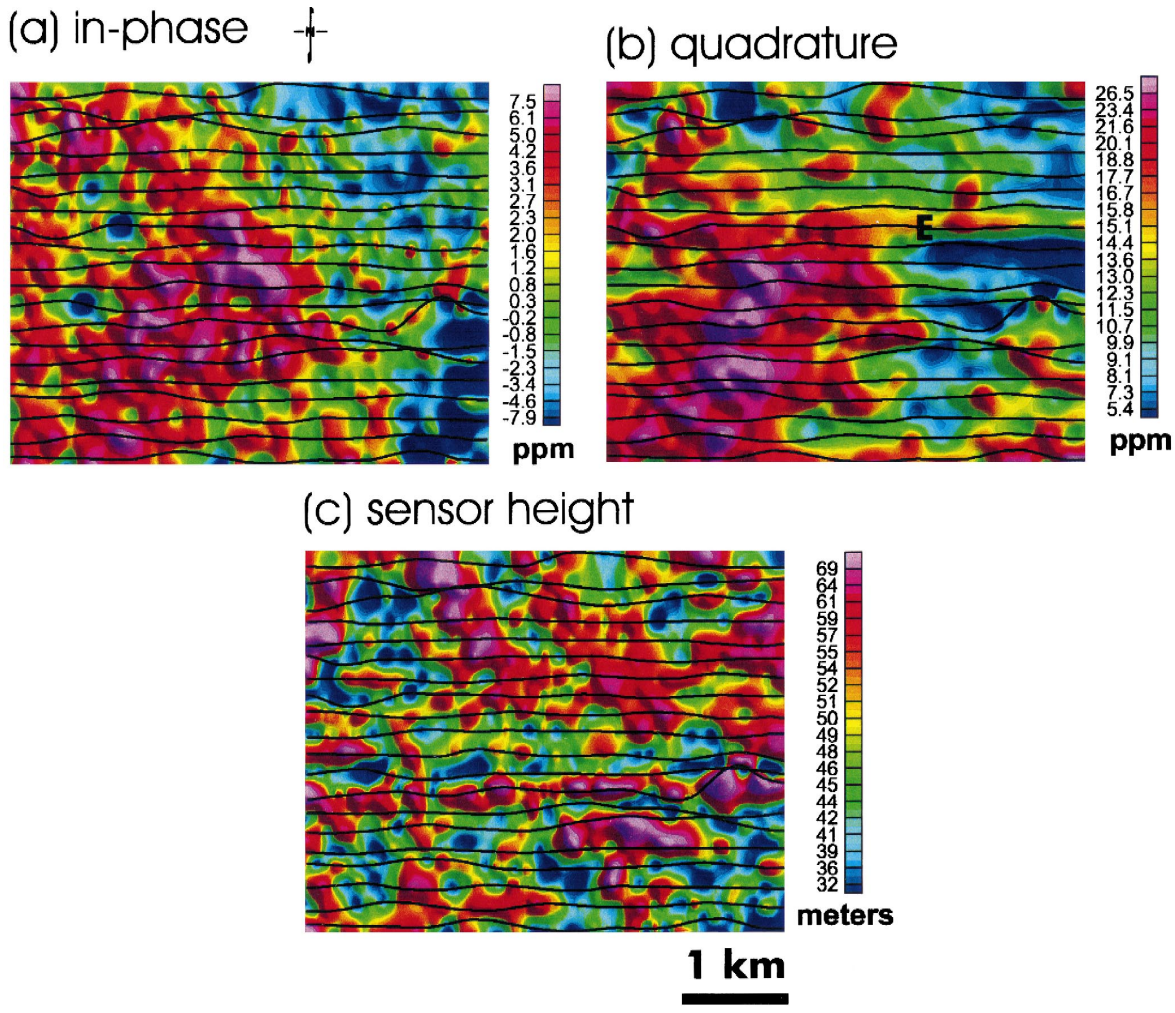


Fig. 10. AEM data over Krokskogen lava flows. Shading is at a 45° sun inclination from the northeast for this and following figures. North is at the top of the figure. (a) In-phase component. (b) Quadrature component. (c) Measured sensor height above ground level.

apparent in the *Q*–IP lookup estimate. In addition, there is a small zone of high conductivity in this same area that does not appear in either of the inversion estimates.

The conductivity pattern from the *Q*–*H* lookup table, shown in Fig. 11d, more closely mimics the quadrature response pattern than does the other methods. The line denoted 'E' in Fig. 10b appears to contain some residual level error in the quadrature component and this error is carried over to the conductivity estimate more than in the estimates of the other methods.

Fig. 11e shows results from a lookup table that is ordered according to ascending IP values (IP–*Q*), but without the correction applied in Eq. (4). The results are almost identical to the results from the commercial IP–*Q* lookup table, shown in Fig. 11f, and are very similar to the *Q*–IP results. The commercial algorithm is not described in the company's documentation, but converts the in-phase and quadrature responses in a more complicated manner than my algorithm, and stores resistivities as log values (H. Wang, personal communication). Evidently, a straightforward approach works as well as more

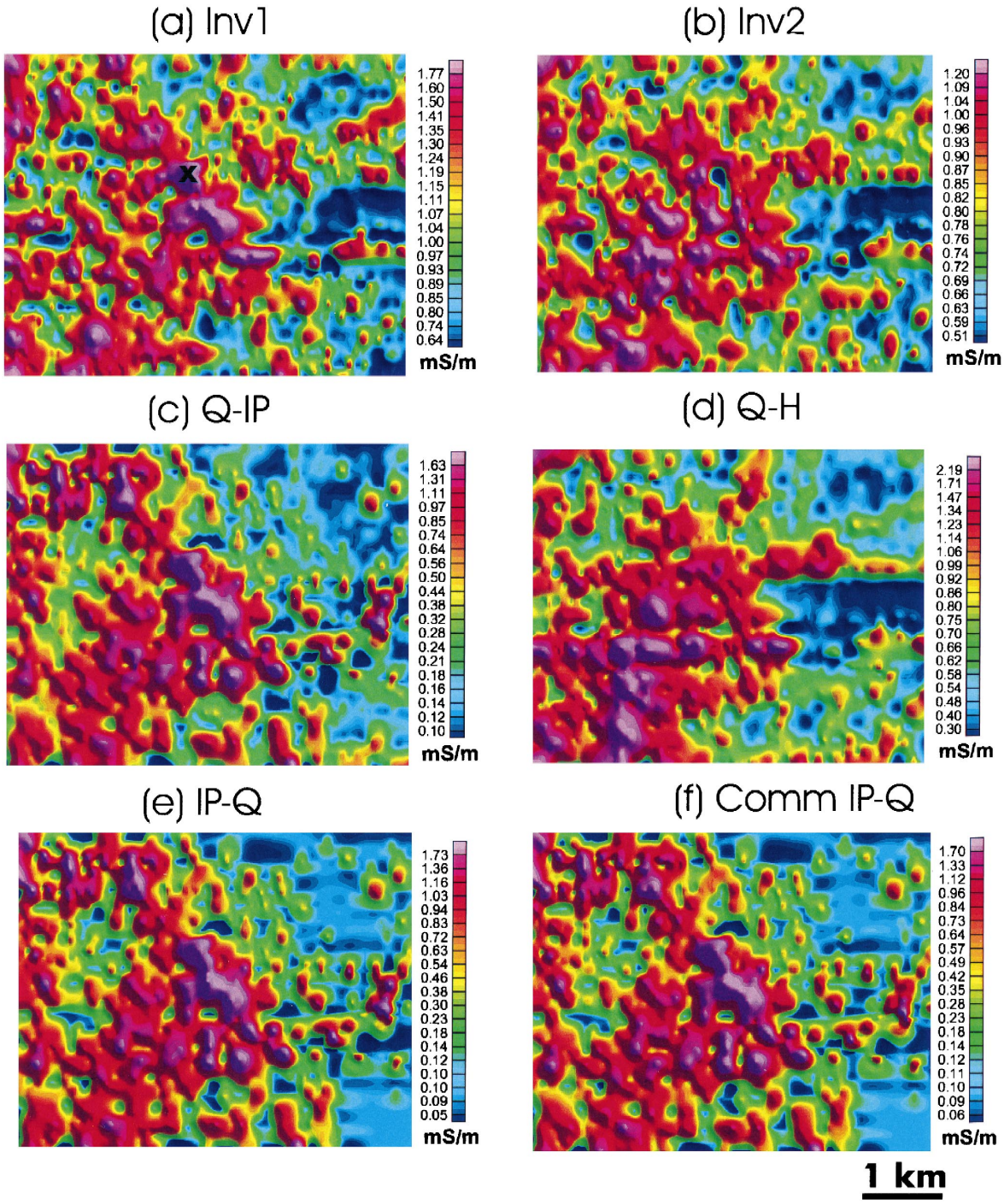


Fig. 11. Earth conductivity estimates of Krokskogen AEM data. (a) Inversion with small allowable sensor height bounds. (b) Inversion using less restrictive sensor height bounds. (c) *Q*–IP lookup table. (d) *Q*–*H* lookup table. (e) IP–*Q* lookup table without Eq. (4) correction. (f) Commercial IP–*Q* lookup table.

complicated schemes, though the latter may have advantages in terms of speed and storage. Furthermore, the commercial IP–*Q* algorithm does not return estimates when either the in-phase or the quadrature response is negative. Over rocks that are fairly resistive or magnetic, even carefully leveled data can have many negative values, and the inability to return a value can mean that large swaths may have no conductivity estimate at all. Zones with no returned conductivity estimates were interpolated using a linear interpolator. This effect is manifest by linear low conductivity stripes on the right side of Fig. 11f. These stripes are also apparent in the IP–*Q* results in Fig. 11e because the rule governing negative IP values for this algorithm requires that that the maximum lookup table resistivity is returned.

The conductivity estimate shown in Fig. 10e did not use the empirical correction given in Eq. (4). With the correction applied, the conductivity pattern, shown in Fig. 12, differs considerably with those in Fig. 11a–f. The conductivity estimates in the east are considerably higher than the other estimates and the

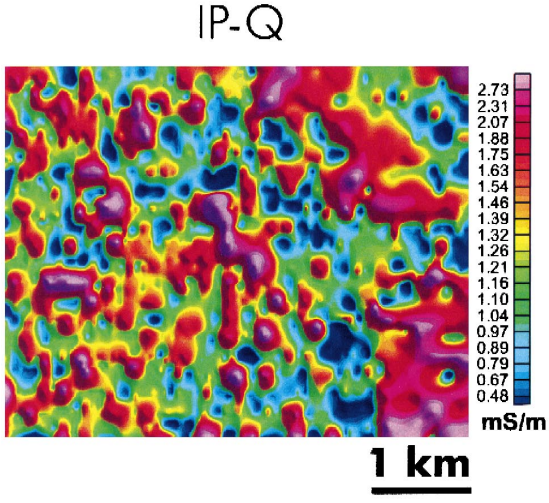


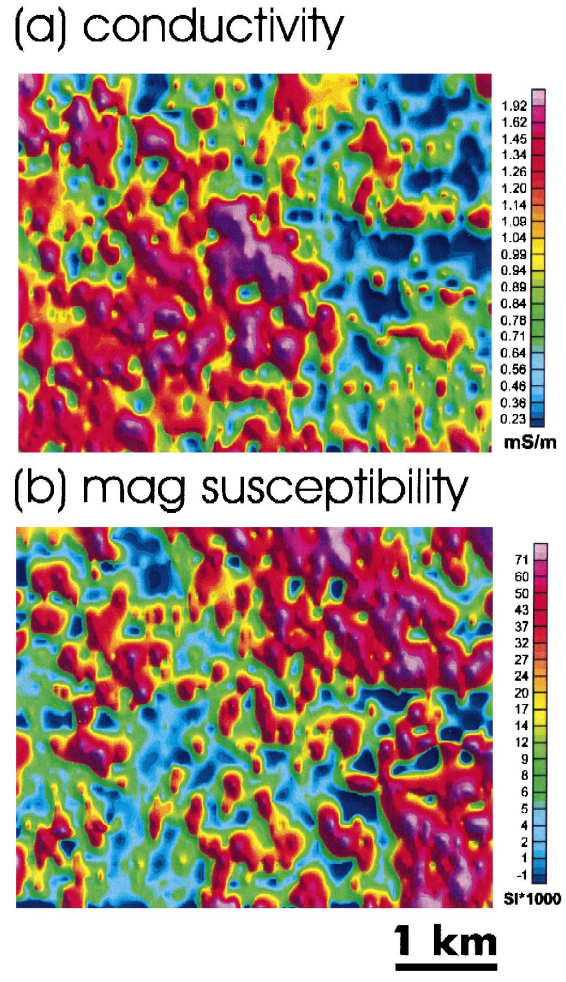


Fig. 12. Erroneous earth conductivity estimates of Krokskogen AEM data using IP–*Q* lookup table with Eq. (4).

Fig. 13. Estimates of Krokskogen AEM data using a magnetic earth IP–*Q* lookup table. (a) Conductivity estimate. (b) Magnetic susceptibility estimate.

conductive zone trending to the SW from near the center of the area does not appear in Fig. 11f. The high conductivity zones in the east are a result of negative in-phase responses in this area combined with moderate quadrature responses. The IP–*Q* table finds in-phase components that yield high resistivities, but the normalization applied via Eq. (4) lowers the estimated resistivities and yields erroneous results. The same problem does not occur if the table is ordered according to the *Q* response. If the *Q*–IP table is used, as in Fig. 11c, the search first finds the moderate (and positive) *Q* response, then searches a range of values in the vicinity, arriving at an appropriately high resistivity even with the application of Eq. (4). In the more rare event of a negative *Q*, the search begins with the lowest positive *Q* values at the start of the table, and a high resistivity is returned.

Field studies by Beard et al. (1997) and Beard and Elvebakk (1999) on the Krokskogen lava flows show considerable variability in magnetic susceptibility. Susceptibilities range from nearly zero to 0.05 SI units with a median susceptibility of about 0.01 SI units. A susceptibility of 0.01 SI units is sufficient to reduce the IP component of System A by about 12 ppm at a 30-m sensor height. Over a sufficiently resistive magnetic earth, the reduced IP component will be negative. Negative values can be seen in the IP response on the east (right) side of the area in Fig. 10a. By using a forward half-space solution that includes non-zero magnetic susceptibility, it is possible to generate a single *Q*–IP lookup table that accounts for variations in magnetic susceptibility as well as resistivity (Huang and Fraser, 2000). As with the *Q*–IP lookup table for a non-magnetic earth, the table is ordered according to increasing *Q* response. However, the six different magnetic susceptibilities will make a table six times larger than the non-magnetic equivalent, and therefore reduce the speed of the lookup procedure, but even so it will only require a few minutes or tens of minutes to process an entire survey. When the closest fitting *Q*–IP pair is found for a particular measurement, the table returns not just resistivity and sensor height estimates, but magnetic susceptibility also. Shown in Fig. 13a is the conductivity estimate based on a magnetic earth *Q*–IP lookup table. The six susceptibilities used in the table ranged from 0.0 to 0.1 SI units, covering the observed range of values in the Krokskogen area. The conductivity pattern is similar to that of the non-magnetic equivalent (Fig. 11c) with some minor but potentially important differences. The conductive feature on the center right of Fig. 11c is absent in Fig. 13a, and Fig. 13a has more conductive areas in the top right quadrant than does Fig. 11a.

The magnetic susceptibility estimated from the lookup table is shown in Fig. 13b. This figure shows a band of high magnetic susceptibility on the east (right) side of the area trending roughly northwest to southeast. The direction is consistent with dominant structural features in the area, and the susceptibility increase from west to east is consistent with both ground susceptibility measurements and aeromagnetic measurements (Beard and Rønning, 1997).

## 6. Discussion and conclusions

The earth is inherently three-dimensional, full of faults and folds, irregular boundaries, magnetic layers, and anisotropic zones. It is a little surprising when methods that use a single frequency of AEM data and approximate the 3-D earth as a flat, non-magnetic, electrically homogeneous half-space work as well as they do. Yet, as numerous case studies have shown, resistivity and conductivity maps made using the half-space approximation consistently image good conductors, faults, fractures, and geological boundaries, and have proved extremely valuable in solving geological problems. However, based on the preceding examples, it is clear that maps based on the half-space approximation have the potential to be over-interpreted. Although the same general conductivity pattern is shown in the maps in Fig. 11a–e, details vary significantly. Extreme topography has an effect on all the methods, but the *Q–H* method appears more susceptible to topographic variation than either the *Q*–IP method or least-squares inversion. In particular, narrow valleys may appear as conductive zones on *Q–H* produced maps. Very good conductors may produce a weak quadrature response, making them almost undetectable on *Q–H* method resistivity maps. However, the IP–*Q* method appears to give reasonably high conductivity estimates over high conductivity structures.

Table 1
Characteristics of resistivity estimation methods

| Statement | Inv | *Q*–IP | *Q*–*H* |
|---|---|---|---|
| Method yields reasonable resistivity estimates over very good conductors. | 2 | 3 | 1 |
| Magnetic rocks or soils do not affect resistivity estimates. | 1 | 1 | 3 |
| Method is unaffected by strong topographic relief. | 2 | 2 | 1 |
| Method yields smooth resistivity estimates along a line. | 1 | 1 | 3 |
| Range of solutions is easily constrained. | 3 | 2 | 2 |
| Method yields information helpful in identifying 3D effects. | 3 | 2 | 1 |
| Method is unaffected by negative or poorly leveled in-phase component. | 2 | 1 | 3 |
| Method allows estimate to depth of conductor beneath resistive overburden. | 3 | 2 | 1 |
| Time to process a typical survey is a few minutes. | 1 | 3 | 3 |

3 = usually true; 2 = sometimes true; 1 = usually false.

An earth having high magnetic susceptibility can result in lookup table or inversion estimates, usually causing resistivity estimate to be too high. However, as was shown in Fig. 13, it is possible to incorporate magnetic susceptibility into a lookup table and get reasonable results.

Earth resistivity has been the principal focus of this paper; however, the use of sensor height estimates as an interpretive tool can be important in some situations. If the geology is such that bedrock is overlain by relatively resistive overburden, the sensor height estimate $H_{est}$ will be greater than the measured sensor height $H$. Thus, the difference in the two quantities yields an estimate of the thickness of the resistive overburden. This can be done using least-squares inversion or the IP–$Q$ lookup method, but is not possible with the $Q$–$H$ lookup method because in this case the sensor height is considered exact. Typically, $H_{est}$ will be larger than $H$; however, over an earth having moderate-to-high magnetic susceptibility, $H_{est}$ can be less than $H$ (Beard and Nyquist, 1998).

Table 1 summarizes the characteristics of the half-space approximation methods. The statements in the table have been worded in such a way that '3' is the desired designation and '1' the poorest. If the columns are summed, there is not much difference between the three methods. In fact, of the three methods described, there is not really a 'best' one. For a given survey, the method that will work best depends on the answer to a number of questions. Are the in-phase measurements reliable? Does prior knowledge about the survey area help to constrain the subset of possible solutions? Is the rock or soil magnetic? The answers to these and other questions help to determine the best method to use.

## Acknowledgements

The Krokskogen helicopter data were collected by John Mogaard and Oddvar Blokkum, employees of the Geological Survey of Norway. Jernbaneverket and the Geological Survey of Norway jointly funded the collection of the field data shown in this paper. Niels B. Christensen, Louise Pellerin, and an anonymous reviewer provided valuable comments that improved the manuscript.

## References

Ahl, A., Winkler, E., Seiberl, W., 1999. Case study of neural network interpretation of airborne electromagnetic measurements. 61st EAGE Conference and Technical Exhibition, Expanded Abstract 2-26.

Beard, L.P., Elvebakk, H., 1999. Geophysical investigations: Krokskogen, Oppkuven, and Gran, 1998. Geological Survey of Norway Report 99.027, 32 pp.

Beard, L.P., Nyquist, J.E., 1998. Simultaneous inversion of airborne electromagnetic data for resistivity and magnetic permeability. Geophysics 63, 1556–1564.

Beard, L.P., Rønning, S., 1997. Data acquisition and processing report—helicopter survey, Krokskogen. Geological Survey of Norway Report 97.134, 9 pp.

Beard, L.P., Lutro, O., Nordgulen, Ø., Siedlecka, A., 1997. Geological and geophysical investigations at Ringerike and Krokskogen (in Norwegian). Geological Survey of Norway Report 97.153, 22 pp.

Everdingen, R.O.V., 1960. Studies in the igneous rock complex of the Oslo region. XVII, Palaeomagnetic analysis of Permian

extrusives in the Oslo region, Norway. Skrifter-Norske Videnskapos Akademi i Oslo, 80 pp.

Fraser, D.C., 1981. Magnetite mapping with a multicoil airborne electromagnetic system. Geophysics 46, 1579–1593.

Frischknecht, F., Labson, V., Spies, B., Anderson, W., 1991. Chapter 3, Profiling methods using small sources. In: Nabighian, M. (Ed.), Electromagnetic Methods in Applied Geophysics—Applications. SEG Investigations in Geophysics No. 3 vol. 2, pp. 105–270.

Hogg, R.L.S., Boustead, G.A., 1990. Estimation of overburden thickness using helicopter electromagnetic data. In: Fitterman, D. (Ed.), Developments and Applications of Modern Airborne Electromagnetic Surveys. U.S. Geol. Surv. Bull. vol. 1925, pp. 103–116.

Huang, H., Fraser, D.C., 2000. Airborne resistivity and susceptibility mapping in magnetically polarizable areas. Geophysics 65, 502–511.

Larsen, B.T., 1978. Krokskogen lava area. In: Dons, J.T., Larsen, B.T. (Eds.), The Oslo Paleorift: A Review and Guide to Excursions. Geological Survey of Norway Bulletin vol. 337, pp. 143–162.

Marquardt, D., 1963. An algorithm for least-squares estimation of nonlinear parameters. J. Soc. Ind. Appl. Math. 11, 431–441.

Menke, W., 1984. Geophysical Data Analysis: Discrete Inverse Theory. Academic Press, Orlando, FL.

Mitsuhata, Y., 2000. 2-D electromagnetic modeling by finite-element method with a dipole source and topography. Geophysics 65, 465–475.

Palacky, G.J. (Ed.) 1986. Airborne Resistivity Mapping. Pap. - Geol. Surv. Can. vol. 86-22.

Press, W., Flannery, B., Teulkolsky, S., Vettering, W., 1992. Numerical Recipes in Fortran—The Art of Scientific Computing. 2nd edn. Cambridge Univ. Press, New York City.

Telford, W.M., Geldart, L.P., Sheriff, R.E., 1990. Chapter 7—Electromagnetic methods. Applied Geophysics. 2nd edn. Cambridge Univ. Press, New York City.

Wait, J.R., 1982. Chapter 3, Electromagnetic induction and loop–loop coupling. Geo-Electromagnetism. Academic Press, New York City.

Ward, S.H., 1961. The electromagnetic response of a magnetic iron ore deposit. Geophys. Prospect. 9, 191–202.